

Finding cool subdwarfs using a $V - J$ reduced proper-motion diagram: Stellar parameters for 91 candidates

David Yong and David L. Lambert

Department of Astronomy, University of Texas, Austin, TX 78712

tofu,dll@astro.as.utexas.edu

ABSTRACT

We present the results of a search for cool subdwarfs for which our candidates were drawn from a $V - J$ reduced proper-motion diagram constructed by Salim & Gould (2002). Kinematic (U, V, and W) and self-consistent stellar parameters (T_{eff} , $\log g$, $[\text{Fe}/\text{H}]$, and ξ_t) are derived for 91 candidate subdwarfs based on high resolution spectra. The observed stars span $3900\text{K} < T_{\text{eff}} < 6200\text{K}$ and $-2.63 < [\text{Fe}/\text{H}] < 0.25$ including only 3 giants ($\log g < 4.0$). Of the sample, 77 stars have MgH lines present in their spectra. With more than 56% of our candidate subdwarfs having $[\text{Fe}/\text{H}] \leq -1.5$, we show that the $V - J$ reduced proper-motion diagram readily identifies metal-poor stars.

Subject headings: stars: abundances – stars: fundamental parameters – subdwarfs

1. Introduction

The chemical history of our Galaxy has been the target of numerous theoretical and observational studies for many decades. Much progress has taken place where the large and increasing body of observed stellar abundances (e.g., Edvardsson et al. 1993; McWilliam et al. 1995; Ryan et al. 1996; Reddy et al. 2003) is complemented by the ongoing refinement of Galactic chemical evolution models (e.g. Timmes et al. 1995; Goswami & Prantzos 2000; Alibés et al. 2001). The ultimate objective of Galactic chemical evolution studies is to be able to predict accurately elemental and isotopic abundances for any given location and time. The spectra of cool stars show molecular bands from which measurements of isotopic abundance ratios can be made (e.g., Mg from MgH, Ti from TiO). These isotopic ratios offer a unique opportunity to test models of Galactic chemical evolution since different stellar sites and nucleosynthetic processes may be responsible for production of the individual isotopes.

Comparing the observed and predicted evolution of isotopic abundances will test aspects of the contributions of stellar nucleosynthesis to Galactic chemical evolution in a way that is just not possible with elemental abundances. In order to measure isotopic ratios from molecular lines, cool subdwarfs (unevolved metal-poor stars that are located below the solar-metallicity main sequence in color-magnitude diagrams) must first be found.

Previous studies such as Ryan (1989) and Carney et al. (1994) drew candidate subdwarfs from proper-motion catalogs and were successful in identifying large numbers of metal-poor stars. Subsequent detailed abundance analyses were carried out on these targets. Both studies focused upon warmer targets, neglecting cooler subdwarfs. Objective prism surveys which identify metal-poor stars by the weakening of Ca II H and K have also been successful in identifying considerable numbers of metal-poor stars (e.g., Bond 1970; Beers et al. 1992; Christlieb 2000). Without a reliable temperature estimate, a cool metal-poor star will have Ca II lines comparable to a warmer metal-rich star thereby biasing the sample towards warmer stars. Numerous stars of spectral type M and later have recently been identified (e.g., Delfosse et al. 1999, Hawley et al. 2002, Reid & Cruz 2002). However, the overwhelming majority of these cool stars are solar metallicity. Only a handful of metal-poor stars with spectral type M or later have been found (e.g., Gizis 1997, Schweitzer et al. 1999, Lépine et al. 2003, and Burgasser et al. 2003). Our target stars are cooler than those found by Ryan (1989) and warmer than those found by Gizis (1997).

In Paper I (Yong & Lambert 2003), we presented the results from our first search for cool subdwarfs. From these subdwarfs we have measured the evolution of the Mg isotopic ratios, extending the Gay & Lambert (2000) measurements to $[\text{Fe}/\text{H}] = -2.5$ (Yong & Lambert in prep). In this paper, we present the results from our second search for cool subdwarfs, self-consistent stellar (T_{eff} , $\log g$, $[\text{Fe}/\text{H}]$, and ξ_t) and kinematic (U, V, W) parameters for a further 91 candidates.

2. Selection criteria

In Paper I, our goal was to identify subdwarfs with $T_{\text{eff}} < 4700\text{K}$ and $[\text{Fe}/\text{H}] < -1.5$, that is, metal-poor stars with MgH molecular features. Following Ryan (1989), we drew candidates from the New Luyten Two-Tenths (NLTT) catalog of stars with annual proper-motions in excess of $0''.18/\text{year}$ (Luyten 1979,1980; Luyten & Hughes 1980). We used the reduced proper-motion criterion to ensure that the selected stars had large transverse velocities relative to the local standard of rest. Since halo stars are on plunging orbits, they are over-represented in proper-motion catalogs. Hertzsprung first introduced the concept of the reduced proper-motion, defined as $H = V + 5 \log \mu + 5$, where V is the apparent magnitude

and μ is the proper-motion in arcsec/year. The reduced proper-motion can also be expressed as $H = M_V + 5 \log \nu_T - 3.37$ where M_V is the absolute magnitude and ν_T is the transverse velocity in km/s. At a given spectral type, a reduced proper-motion constraint rejects stars whose transverse velocities fall below a chosen value. Subdwarfs are less luminous than disk dwarfs at a given color and have larger transverse velocities. Both of these factors lead to an increase in the reduced proper-motion of the subdwarf population relative to the disk dwarf population. While our original search, Paper I, was successful in finding these subdwarfs, our efficiency was less than ideal. Of our 134 candidates, only 11 stars had $[\text{Fe}/\text{H}] < -1.5$ and MgH lines.

For this search, we again utilized the reduced proper-motion criterion to identify metal-poor stars drawn from the NLTT catalog. Instead of relying upon Luyten’s original photometry, we made use of the excellent work by Salim & Gould (2002, 2003) and Gould & Salim (2003). Salim & Gould cross-referenced the NLTT catalog with 2MASS (Skrutskie et al. 1997) and USNO-A (Monet et al. 1998) to obtain optical and infrared photometry. Proper-motions were determined from the difference in positions between the two catalogs. Salim & Gould (2002) then constructed an optical-infrared reduced proper-motion diagram from which they identify “distinct tracks for white dwarfs, subdwarfs, and main-sequence stars”. A reduced proper-motion diagram based on the original Luyten photometry does not show the expected separation between subdwarfs and main-sequence stars. Salim & Gould suggest that the reduced proper-motion diagram based on the original Luyten photometry suffers from a “short color baseline and large errors”. In Paper I, we confirmed the Ryan (1989) statement that the photometric “values tabulated in the NLTT catalog must be regarded as approximate only”. Another advantage of the optical-infrared reduced proper-motion diagram is that the colors provide an accurate estimate of the effective temperature. In Figure 1, we show a reduced proper-motion diagram identical to that of Salim & Gould with one exception. Rather than using $V + 5 \log \mu$, we use $J + 5 \log \mu$ as the reduced proper-motion. The rationale is that the 2MASS photometry is more accurate than USNO. Using photographic plates, the principal objective of the USNO catalog is astrometry while the photometry is a by-product. USNO-A provides B_U and R_U magnitudes which are converted to V according to the relation given in Salim & Gould (2000) $V = R_U + 0.23 + 0.32(B - R)_U$. Salim & Gould (2003) show that the uncertainties in V are around 0.25 mag while uncertainties in J are around 0.02 mag. However, there are no discernable differences between the original ($V + 5 \log \mu$) reduced proper-motion diagram and ours ($J + 5 \log \mu$). The locations of white dwarfs, subdwarfs, and main-sequence stars (solar metallicity) can be easily estimated.

Of the stars we observed in Paper I, a subset had optical and infrared photometry from Salim & Gould (2002, 2003). After constructing a reduced proper-motion diagram, we overplotted the stars we observed in Paper I. It was clear that the metal-poor stars

were separated from the metal-rich stars. For this search, we selected stars with $H_J \geq 4 + 2 \times (V - J)$ where $H_J = J + 5 \log \mu$ with V and J taken from Salim & Gould (2002, 2003). This cutoff was the approximate line dividing the subdwarfs from the main sequence stars studied in Paper I. To ensure we observed cool stars, we generally observed targets which had $1.4 < V - J < 2.6$. The magnitude limit was $V \leq 13.9$, the limit of the McDonald 2.7m telescope. We also imposed a declination limit $-40^\circ \leq \delta \leq 90^\circ$ appropriate for McDonald observatory. This resulted in a list of 470 candidate subdwarfs.

In Paper I, the most metal-poor star we observed which showed MgH lines was G39-36, $T_{\text{eff}}=4200\text{K}$ and $[\text{Fe}/\text{H}]=-2.5$. Not only did this star have a large reduced proper-motion, it was also marked by a large ultraviolet excess, $\delta(U - B)_{0.6} = 0.25$ (Sandage & Kowal 1986). Roman (1955) found a correlation between the ultraviolet excess and the strength of metallic lines in high velocity stars. Schwarzschild et al. (1955) showed that a lower metal abundance and the corresponding reduction in line blanketing was responsible for the ultraviolet excess (see also Carney 1979 and references within). Therefore, we also observed cool stars with large ultraviolet excesses taken from Sandage & Kowal (1986). Finally, bright solar metallicity stars expected to have strong MgH lines were also added to the list of candidates to be observed. These bright stars were taken from the HIPPARCOS catalog (ESA 1997) and from Carney et al. (1994). In total we observed 91 targets; 58 selected from the $V - J$ reduced proper-motion diagram, 24 bright targets, and 9 from (Sandage & Kowal 1986).

3. Observations and data reduction

Table 1 contains the list of candidates observed at McDonald Observatory on the 2.7m Harlan J. Smith telescope between September 2002 and February 2003. The data were obtained using the cross-dispersed echelle spectrometer (Tull et al. 1995) at the coudé f/32.5 focus with a resolving power of either 30,000 or 60,000. The detector was a Tektronix CCD with $24 \mu\text{m}^2$ pixels in a 2048×2048 format. Using this setting, the spectral coverage was from 3800\AA to 8900\AA with gaps between the orders beyond 5800\AA . These observations incorporated the MgH $A - X$ lines near 5140\AA . Visual inspection of the data indicated the presence or absence of MgH molecular features. Of our sample of 91 stars, 14 stars did not show MgH lines and 77 stars showed MgH lines. Numerous Fe I and Fe II lines were available in the observed spectra for spectroscopic determination of the stellar parameters. For each star, exposure times were generally 20-30 minutes and multiple exposures were taken and co-added to increase the signal-to-noise ratio when necessary. Although varying from star to star, the typical signal-to-noise ratio of the extracted one dimensional spectra was 60 per

pixel at 6500Å. One dimensional wavelength calibrated normalized spectra were extracted in the standard way using the IRAF¹ package of programs. Equivalent widths were measured using IRAF where in general Gaussian profiles were fit to the observed profile.

4. Analysis

4.1. Deriving stellar parameters

We determined the stellar parameters using the same method described in Paper I. The local thermodynamic equilibrium (LTE) stellar line analysis program MOOG (Snedden 1973) was used in combination with the adopted model atmosphere. For $\log g > 3.5$, we used the NEXTGEN model atmosphere grid for low mass stars computed by Hauschildt et al. (1999). For giants with $\log g \leq 3.5$ we used LTE model atmospheres computed by Kurucz (1993). In both cases we interpolated within the grid when necessary. Equivalent widths (EWs) of 35 Fe I lines and 5 Fe II lines were measured. The gf values of the lines were taken from Lambert et al. (1996) and from a compilation by R.E. Luck (1993, private communication). The effective temperature (T_{eff}) was set by insisting that the abundances of individual Fe lines be independent of lower excitation potential. Ideally, the Alonso et al. (1996, 1999) $T_{\text{eff}}:[Fe/H]:color$ relations based on the infrared flux method would be used to obtain values for T_{eff} . In particular, the $(V - K)$ color provides the greatest accuracy. Unfortunately, for $[Fe/H] \leq -1.5$, the Alonso et al. (1996) $(V - K)$ relation is only applicable above $T_{\text{eff}} \simeq 4600\text{K}$ and Salim & Gould (2003) have shown that errors in V are 0.25 mag. The microturbulence (ξ_t) was set by requiring that the abundances of individual Fe lines show no trend against equivalent width. By forcing agreement between the Fe abundance derived from neutral and ionized lines, the gravity ($\log g$) was fixed. This process required iteration until a consistent set of parameters were obtained (see Figure 2) from which the Fe abundance was determined from the mean of all Fe lines.

Only weak lines, EWs $< 90 \text{ m}\text{\AA}$, were used in the analysis if possible. We observed the solar spectrum at $R=60,000$ to check our analysis techniques. We measured 30 Fe I lines and 7 Fe II lines and compared our equivalent widths with the Grevesse & Sauval (1999) values. Our equivalent widths were larger by a mean value of $3.7 \text{ m}\text{\AA}$ with a standard deviation of $2.6 \text{ m}\text{\AA}$. We note that our equivalent widths were measured from a disk integrated solar spectrum whereas the Grevesse & Sauval (1999) equivalent widths were measured at disk

¹IRAF is distributed by the National Optical Astronomy Observatories, which are operated by the Association of Universities for Research in Astronomy, Inc., under cooperative agreement with the National Science Foundation.

center from the Delbouille et al. (1973) solar atlas. Using our equivalent widths and a NEXTGEN model atmosphere, we derived a solar abundance of $\log\epsilon(\text{Fe})= 7.54$. Considering the Grevesse & Sauval (1999) value of $\log\epsilon(\text{Fe})= 7.50 \pm 0.05$ derived from their empirical model solar atmosphere, we adopted $\log\epsilon(\text{Fe})= 7.52$ as the solar Fe abundance for this study.

The derived model parameters have uncertainties which were estimated in the following way. We varied T_{eff} until the trends between lower excitation potential and abundance were unacceptable. Likewise, we changed the microturbulence until the trends between equivalent width and abundance were poor. The gravity was adjusted until the difference between the abundance from Fe I and Fe II lines was greater than the standard deviation of the Fe abundance derived from Fe I lines (typically 0.1–0.15 dex). Estimated uncertainties in the model parameters are $\delta T_{\text{eff}}=150\text{K}$, $\delta\log g=0.3$ dex, $\delta\xi_t=0.3$ km s⁻¹, and $\delta[\text{Fe}/\text{H}]=0.2$ dex. Though the targets were fainter than those in Paper I, we increased the number of exposures to ensure the signal-to-noise ratio was similar. And so the uncertainties in the model parameters are identical to those in Paper I.

4.2. Comparison with literature

A search on SIMBAD indicated that 10 stars had previously determined temperatures and 17 stars had previously determined metallicities. In Table 2, we compare our values with those found in the literature. Combining our data with Paper I, we find a mean offset $\langle T_{\text{eff}}(\text{Yong \& Lambert}) - T_{\text{eff}}(\text{literature}) \rangle = -16$ K with a standard deviation of 115K (see Figure 3). Again combining our data with Paper I, the mean offset is $\langle [\text{Fe}/\text{H}] (\text{Yong \& Lambert}) - [\text{Fe}/\text{H}] (\text{literature}) \rangle = -0.06$ dex with a standard deviation of 0.38 dex (see Figure 4). There is a reasonable agreement between the stellar parameters derived in this study (and Paper I) and the values found in a variety of sources in the literature.

4.3. Self-consistency check

Molecular lines will not be visible in the spectra of stars with sufficiently high temperatures and/or low abundances. A simple self-consistency test of our stellar parameters is to predict the limit in temperature and metallicity at which molecular lines will not be observed. Once a detection limit is obtained, we can then check the stellar parameters to determine whether molecular lines should or should not be present. We synthesized representative MgH and TiO lines assuming a resolving power of 60,000 and $\log g = 4.5$. The MgH molecular data were taken from Gay & Lambert (2000) while the TiO molecular data were taken from

Jørgensen (1994). Values of $[\text{Ti}/\text{Fe}]$ and $[\text{Mg}/\text{Fe}]$ in accord with observed trends summarized in Alibés et al. (2001) were assumed, i.e., $[\text{Mg}/\text{Fe}]=0.4$ at $[\text{Fe}/\text{H}]=-1.5$. At a given value for T_{eff} , we decreased the metallicity until the molecular features reached a depth of $\sim 5\%$ relative to the continuum. We considered this value of T_{eff} and $[\text{Fe}/\text{H}]$ to be our detection limit. In Figure 5, we plot our stars in temperature–metallicity space imposing our limits of detection for MgH and TiO. At a fixed metallicity, MgH is detectable to considerably higher values of T_{eff} than TiO. Despite TiO (6.9 eV) having a higher dissociation energy than MgH (1.34 eV), the overwhelming H abundance ensures the continuing presence of MgH to higher temperatures.

All 14 stars that show neither MgH nor TiO lines occupy a region in temperature–metallicity space where, for the given stellar parameters, we would not expect to see molecular lines. All 77 stars that show MgH lines lie in the region where, for the given stellar parameters, we do expect to see molecular lines. Our approximate limits of detection assume a resolving power of 60,000 and $\log g = 4.5$. For objects observed at a lower resolving power, we expect the detection limit would move to lower values of T_{eff} at a fixed metallicity. Likewise, the detection limit for giants would be shifted to lower values of T_{eff} at a fixed metallicity. The vast majority of the stars observed in Paper I also lie in the expected regions. That is, stars with MgH lines lie to the left of the detection limit while stars without MgH lines fall to the right of the detection limit in Figure 5. We note that the handful of stars that do not conform to the predictions are observed at lower resolving powers or are giants. Through the synthesis of representative molecular lines, we have performed a self-consistency check validating our derived stellar parameters.

5. Discussion

5.1. Kinematics

We used the reduced proper-motion constraint to select stars kinematically distinct from the thin disk. This selection criterion was used in order to observe stars on halo-like orbits with halo-like metallicities. The first check we can implement is to determine whether we successfully targeted stars with kinematics unlike thin disk stars. Following the Johnson & Soderblom (1987) recipe, we calculated the Galactic space-velocity components U (positive towards the Galactic center), V (positive in the direction of Galactic rotation), and W (positive towards the north Galactic pole) along with the associated uncertainties σ_U , σ_V , and σ_W (see Table 1). For the solar motion with respect to the local standard of rest (LSR), we assumed the Dehnen & Binney (1998) values (+10,+5,+7) km s^{-1} in (U,V,W). Note that in Paper I, we incorrectly applied a correction of -10 km s^{-1} in U . Therefore, $+20 \text{ km s}^{-1}$

must be added to our values of U in Paper I to obtain U_{LSR} . In the absence of HIPPARCOS parallaxes, spectroscopic parallaxes were determined by using the derived model parameters and the Y^2 isochrones (Yi et al. 2001). In Figure 6 we plot U_{LSR} , V_{LSR} , and W_{LSR} versus $[Fe/H]$ including the stars from Paper I. As in Paper I, we identify stars that lag the LSR, $V < -50$ km s $^{-1}$, as likely members of the thick disk or halo. As expected, our reduced proper-motion constraint enabled us to select stars belonging to populations kinematically distinct from the thin disk.

5.2. Metallicity

Our goal was to find stars with $[Fe/H] \leq -1.5$. The second check we can conduct is to verify the success of our selection criteria in targeting metal-poor stars. In Figure 7 we plot the number of stars versus metallicity for this study, Paper I, Carney et al. (1994), and the Ryan & Norris (1991) sample. In Paper I, we noted that our distribution was similar to the Carney sample. We also mentioned that the Ryan sample had a peak at lower metallicity since these stars were observations of metal-poor candidates identified by Ryan (1989) as having an ultraviolet excess corresponding to $[Fe/H] < -1.2$, that is, $\delta(U - B)_{0.6} > 0.2$. In this study, we were far more successful in identifying metal-poor stars with 38 out of 91 stars being more metal-poor than $[Fe/H] = -1.5$. As a comparison, in Paper I we had 27 of 134 stars with $[Fe/H] \leq -1.5$. In this study, 32 stars were more metal-poor than $[Fe/H] = -1.5$ with MgH lines present in their spectra. As a comparison, 11 stars in Paper I were more metal-poor than $[Fe/H] = -1.5$ with MgH lines present in their spectra. Clearly the selection technique utilized in this paper was more successful than the technique applied in Paper I. That is, the Salim & Gould (2002) optical-infrared reduced proper-motion diagram separates subdwarfs from main-sequence stars more effectively than a reduced proper-motion diagram based on the original Luyten photometry.

Let us consider only those stars with 2MASS and USNO photometry, i.e., only the stars in Figure 8. After combining this study with the stars in Paper I, we find that 56% (43 of 76) of stars that lie below the cutoff have $[Fe/H] \leq -1.5$. While this is far from the ultra metal-poor stars currently being discovered by other programs, $[Fe/H] \leq -1.5$ is a metallicity regime in which the Mg isotope ratios have not been explored. In this metallicity range, only cool subdwarfs will show MgH lines. We also note that beyond $J + 5 \log \mu = 10$, all of the observed stars are more metal-poor than $[Fe/H] = -1.5$.

5.3. Temperature

Our goal was to find stars with $T_{\text{eff}} < 4700\text{K}$. More specifically, ideal targets were stars with $[\text{Fe}/\text{H}] < -1.5$ with MgH molecular lines. Of the 91 stars presented in this paper, 38 had $T_{\text{eff}} \leq 4700\text{K}$ and given the uncertainties in our derived effective temperatures, we note that 48 of the 91 stars had $T_{\text{eff}} \leq 4800\text{K}$. As a comparison, in Paper I 44 of the 134 stars had $T_{\text{eff}} < 4700\text{K}$ and 69 of the 134 stars had $T_{\text{eff}} \leq 4800\text{K}$. In Figure 9, we plot the number of stars versus T_{eff} for this study, Paper I, and the Carney et al. (1994) sample. Our temperature distributions are similar between this study and Paper I. Both of our searches have focused upon stars considerably cooler than the Carney study which highlights the different temperature regimes of interest. Importantly, 77 of the 91 stars presented here have MgH lines. In Paper I, 100 of the 134 stars had MgH lines.

In Paper I, we confirmed Ryan’s findings that the Luyten colors were inaccurate. Firstly, the magnitudes were published to only 0.1 mag. Secondly, we chose stars assigned by Luyten to color classes g-k, k, or k-m. These stars spanned $4200\text{K} < T_{\text{eff}} < 6400\text{K}$ yet the Luyten colors for this range of stars were $m_{\text{pg}} - m_R = 0.9, 1.1, \text{ or } 1.3$. We now comment on the colors in the Salim & Gould (2002) study. In Figure 10, we plot the $V - J$ color against our derived temperatures (this study and Paper I) separated into four metallicity bins. This Figure shows that a fair estimate of the effective temperature can be obtained from the $V - J$ color. Alonso et al. (1996, 1999) derived $T_{\text{eff}}: [\text{Fe}/\text{H}]: \text{color}$ relations for dwarfs and giants using the infrared flux method. They have shown that the $V - K$ color index provides the most accurate temperature estimates. (We refrain from using the infrared flux method calibrations due to the uncertainties in V .) In Figure 11, we plot the $V - K$ color against our derived temperatures and find that the dispersion about the mean is slightly less than for $V - J$. The K magnitudes were also from 2MASS and presented by Salim & Gould (2002). This reduced scatter in the $V - K$ versus T_{eff} plot suggests that a reduced proper-motion diagram featuring $V - K$ versus $K + 5 \log \mu$ may be a power tool when the metal-poor targets need to span a small temperature range. In this Figure we also plot the Alonso et al. (1996) $(V - K): T_{\text{eff}}$ relation for dwarfs. We find that this relation reasonably matches our data though at the metal-poor end, our data extend to cooler temperatures than the Alonso et al. (1996) relations. In both the $V - J$ and $V - K$ plots (Figures 10 and 11), we suspect that the dispersion is primarily due to errors in V . Earlier we mentioned that the errors in V were around 0.25 mag while the errors in J (and presumably K) were only 0.02 mag (Salim & Gould 2003). While reddening may also be a factor, we note that these cool dwarfs lie within 100pc of the sun and errors in $V - J$ and $V - K$ would overwhelm any reddening effects.

Based on spectrum synthesis, Cottrell (1978) showed that MgH lines in cool stars can

be a useful metal abundance discriminant. In cool stars, the strength of the MgH lines does not strongly depend on metallicity, unlike atomic lines. For sufficiently cool stars, a decrease in the metal abundance will weaken the atomic lines whilst the MgH lines remain strong. In Figure 12, we show the spectra of 4 stars highlighting some MgH lines and a strong atomic line. In 2 of the spectra the “normal” situation is shown in which the MgH lines are dwarfed by the strong atomic line. In the other 2 spectra, Cottrell’s prediction is verified since the MgH lines are comparable in strength to the atomic line. That is, the atomic line has weakened while the MgH lines have maintained their strength. Note that all stars shown in Figure 12 are very cool. If these stars were solar metallicity, Figure 5 shows that the spectra of these stars would be swamped with TiO lines.

6. Concluding remarks

We present stellar parameters for 91 candidate subdwarfs selected primarily by their large reduced proper-motions. Our goal was to identify metal-poor stars $[\text{Fe}/\text{H}] < -1.5$ with MgH lines. This is the 2nd search that we have conducted for these cool subdwarfs. In our first search, we drew candidates from a reduced proper-motion diagram based on Luyten’s original photometry. While we were able to find cool subdwarfs, our efficiency was low (11 of 134 stars had $[\text{Fe}/\text{H}] < -1.5$ and MgH lines). Errors in the Luyten photometry resulted in a reduced proper-motion diagram without cleanly separated populations of subdwarfs and solar-metallicity main-sequence stars. In this search, we made use of the 2MASS infrared and USNO optical photometry presented by Salim & Gould (2002). The reduced proper-motion diagram based on this photometry showed distinct populations of subdwarfs and main-sequence stars. Spectroscopic observations of these candidate subdwarfs showed that the majority were metal-poor stars. Of the candidate subdwarfs selected from their location in the optical-infrared reduced proper-motion diagram, we have shown that 56% have $[\text{Fe}/\text{H}] < -1.5$. In Paper I, only 20% of candidates had $[\text{Fe}/\text{H}] < -1.5$. Further, we verified that the $V - J$ color index was well correlated with T_{eff} such that cool stars suspected of having MgH lines could be targeted. We intend to make further observations to identify cool subdwarfs. In this search, we found a further 32 stars with $[\text{Fe}/\text{H}] < -1.5$ and MgH lines. We intend to re-observe candidates from this study with higher resolving power and higher signal-to-noise ratio in order to measure the Mg isotope ratios to study Galactic chemical evolution.

We are grateful to Samir Salim and Andy Gould for providing a list of candidate subdwarfs prior to publication. We thank G. Fritz Benedict for valuable discussions and the referee, Andy Gould, for helpful comments. We acknowledge support from the Robert A. Welch Foundation of Houston, Texas. This research has made use of the SIMBAD database,

operated at CDS, Strasbourg, France and NASA's Astrophysics Data System.

REFERENCES

- Alibés, A., Labay, J., & Canal, R. 2001, *A&A*, 370, 1103
- Alonso, A., Arribas, S., & Martínez-Roger, C. 1996, *A&A*, 313, 873
- . 1999, *A&AS*, 140, 261
- Beers, T. C., Preston, G. W., & Shectman, S. A. 1992, *AJ*, 103, 1987
- Bond, H. E. 1970, *ApJS*, 22, 117
- Burgasser, A. J., Kirkpatrick, J. D., Burrows, A., Liebert, J., Reid, I. N., Gizis, J. E., McGovern, M. R., Prato, L., & McLean, I. S. 2003, *ApJ* in press (astro-ph/0304174)
- Carney, B. W. 1979, *ApJ*, 233, 211
- Carney, B. W., Latham, D. W., Laird, J. B., & Aguilar, L. A. 1994, *AJ*, 107, 2240
- Christlieb, N. 2000, Ph.D. Thesis, Univ. of Hamburg
- Cottrell, P. L. 1978, *ApJ*, 223, 544
- Dehnen, W. & Binney, J. J. 1998, *MNRAS*, 298, 387
- Delbouille, L., Roland, G., & Neven, L. 1973, *Photometric Atlas of the Solar Spectrum from 3000 to 10000 Å*. Institut d'Astrophysique, Université de Liège
- Delfosse, X., Tinney, C. G., Forveille, T., Epchtein, N., Borsenberger, J., Fouqué, P., Kimeswenger, S., & Tiphène, D. 1999, *A&AS*, 135, 41
- Edvardsson, B., Andersen, J., Gustafsson, B., Lambert, D. L., Nissen, P. E., & Tomkin, J. 1993, *A&A*, 275, 101
- ESA. 1997, *VizieR Online Data Catalog*
- Gay, P. L. & Lambert, D. L. 2000, *ApJ*, 533, 260
- Gizis, J. E. 1997, *AJ*, 113, 806
- Goswami, A. & Prantzos, N. 2000, *A&A*, 359, 191

- Gould, A. & Salim, S. 2003, *ApJ*, 582, 1001
- Grevesse, N. & Sauval, A. J. 1999, *A&A*, 347, 348
- Hauschildt, P. H., Allard, F., & Baron, E. 1999, *ApJ*, 512, 377
- Hawley, S. L., Covey, K. R., Knapp, G. R., Golimowski, D. A., Fan, X., Anderson, S. F., Gunn, J. E., Harris, H. C., Ivezić, Ž., Long, G. M., Lupton, R. H., McGehee, P. M., Narayanan, V., Peng, E., Schlegel, D., Schneider, D. P., Spahn, E. Y., Strauss, M. A., Szkody, P., Tsvetanov, Z., Walkowicz, L. M., Brinkmann, J., Harvanek, M., Hennessy, G. S., Kleinman, S. J., Krzesinski, J., Long, D., Neilsen, E. H., Newman, P. R., Nitta, A., Snedden, S. A., & York, D. G. 2002, *AJ*, 123, 3409
- Johnson, D. R. H. & Soderblom, D. R. 1987, *AJ*, 93, 864
- Jørgensen, U. G. 1994, *A&A*, 284, 179
- Kurucz, R. 1993, *ATLAS9 Stellar Atmosphere Programs and 2 km/s grid*. Kurucz CD-ROM No. 13. Cambridge, Mass.: Smithsonian Astrophysical Observatory, 1993., 13
- Lépine, S., Shara, M. M., & Rich, R. M. 2003, *ApJ*, 585, L69
- Lambert, D. L., Heath, J. E., Lemke, M., & Drake, J. 1996, *ApJS*, 103, 183
- Luyten, W. J. 1979,1980, *New Luyten Catalogue of Stars with Proper Motions Larger than Two Tenths of an Arcsecond* (Minneapolis: University of Minnesota, 1979,1980)
- Luyten, W. J. & Hughes, H. S. 1980, *Proper Motion Survey with the Forty-Eight Inch Schmidt Telescope. LV. First Supplement to the NLTT Catalogue* (Minneapolis: University of Minnesota, 1980)
- McWilliam, A., Preston, G. W., Sneden, C., & Searle, L. 1995, *AJ*, 109, 2757
- Monet, D. B. A., Canzian, B., Dahn, C., Guetter, H., Harris, H., Henden, A., Levine, S., Luginbuhl, C., Monet, A. K. B., Rhodes, A., Riepe, B., Sell, S., Stone, R., Vrba, F., & Walker, R. 1998, *VizieR Online Data Catalog*
- Reddy, B. E., Tomkin, J., Lambert, D. L., & Allende Prieto, C. 2003, *MNRAS*, 340, 304
- Reid, I. N. & Cruz, K. L. 2002, *AJ*, 123, 2806
- Roman, N. G. 1955, *ApJS*, 2, 195
- Ryan, S. G. 1989, *AJ*, 98, 1693

- Ryan, S. G. & Norris, J. E. 1991, *AJ*, 101, 1835
- Ryan, S. G., Norris, J. E., & Beers, T. C. 1996, *ApJ*, 471, 254
- Salim, S. & Gould, A. 2000, *ApJ*, 539, 241
- . 2002, *ApJ*, 575, L83
- . 2003, *ApJ*, 582, 1011
- Sandage, A. & Kowal, C. 1986, *AJ*, 91, 1140
- Schwarzschild, M., Searle, L., & Howard, R. 1955, *ApJ*, 122, 353
- Schweitzer, A., Scholz, R.-D., Stauffer, J., Irwin, M., & McCaughrean, M. J. 1999, *A&A*, 350, L62
- Skrutskie, M. F., Schneider, S. E., Stiening, R., Strom, S. E., Weinberg, M. D., Beichman, C., Chester, T., Cutri, R., Lonsdale, C., Elias, J., Elston, R., Capps, R., Carpenter, J., Huchra, J., Liebert, J., Monet, D., Price, S., & Seitzer, P. 1997, in *ASSL Vol. 210: The Impact of Large Scale Near-IR Sky Surveys*, 25
- Snedden, C. 1973, *ApJ*, 184, 839
- Timmes, F. X., Woosley, S. E., & Weaver, T. A. 1995, *ApJS*, 98, 617
- Tull, R. G., MacQueen, P. J., Sneden, C., & Lambert, D. L. 1995, *PASP*, 107, 251
- Yi, S., Demarque, P., Kim, Y., Lee, Y., Ree, C. H., Lejeune, T., & Barnes, S. 2001, *ApJS*, 136, 417
- Yong, D. & Lambert, D. L. 2003, *PASP*, 115, 22

Fig. 1.— $V - J$ reduced proper-motion diagram. The points are NLTT stars with 2MASS and USNO-A identifications made by Salim & Gould (2002, 2003). Main-sequence stars (MS) are separated from the subdwarfs (SD) by the solid line. White dwarfs (WD) are separated from SDs and MS stars by the dashed line.

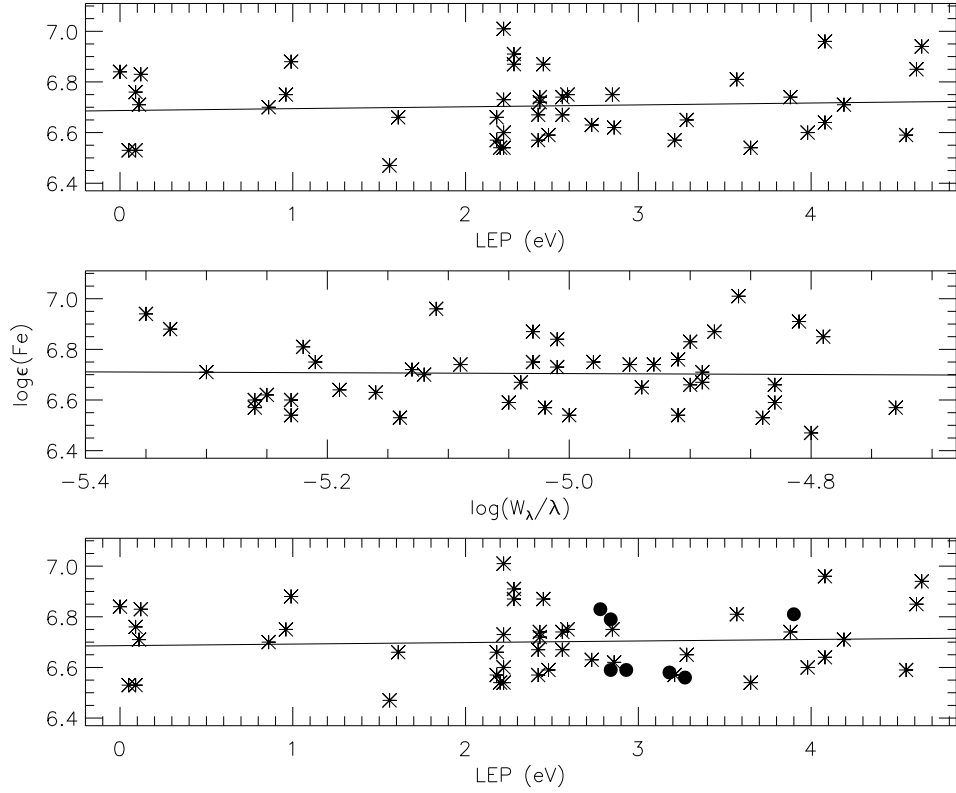


Fig. 2.— Determination of stellar parameters T_{eff} , $\log g$, and ξ_t using excitation and ionization equilibria for G266-8. In the top panel, the lower excitation potential (LEP)-abundance relation is used to set T_{eff} . In the middle panel, the reduced equivalent width (W_λ/λ)-abundance relation is used to determine ξ_t . In the bottom panel, the abundances of Fe I (asterisks) and Fe II (filled circles) are used to fix $\log g$. In all panels the line represents the linear least squares fit to the data.

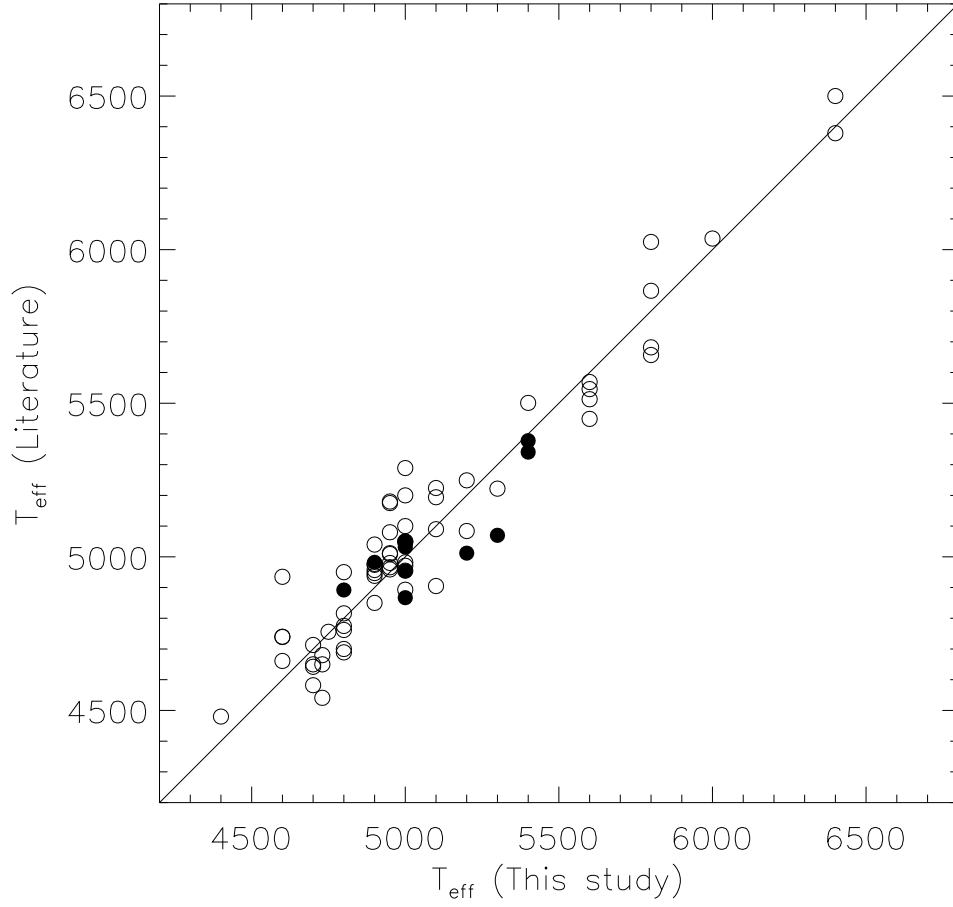


Fig. 3.— T_{eff} comparisons between Yong & Lambert (this study and Paper I) and various literature studies. The open circles represent the data from Paper I while the filled circles are stars from this study. The solid line represents the line of equality.

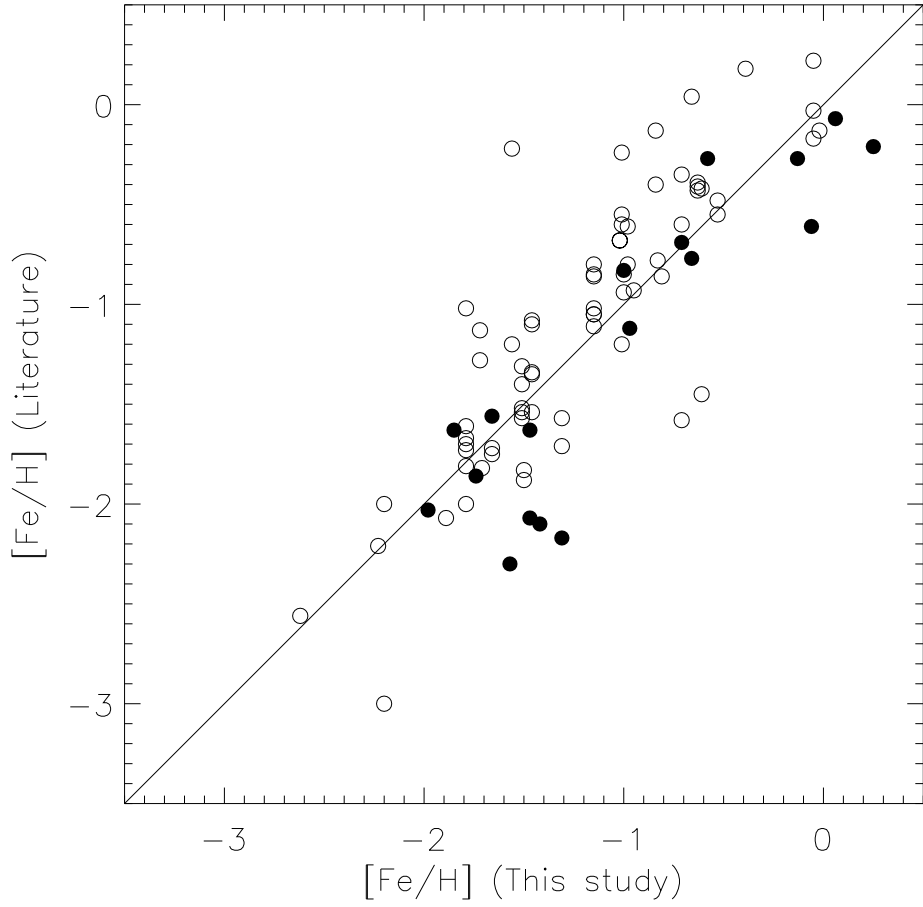


Fig. 4.— $[\text{Fe}/\text{H}]$ comparisons between Yong & Lambert (this study and Paper I) and various literature studies. The open circles represent the data from Paper I while the filled circles are stars from this study. The solid line represents the line of equality.

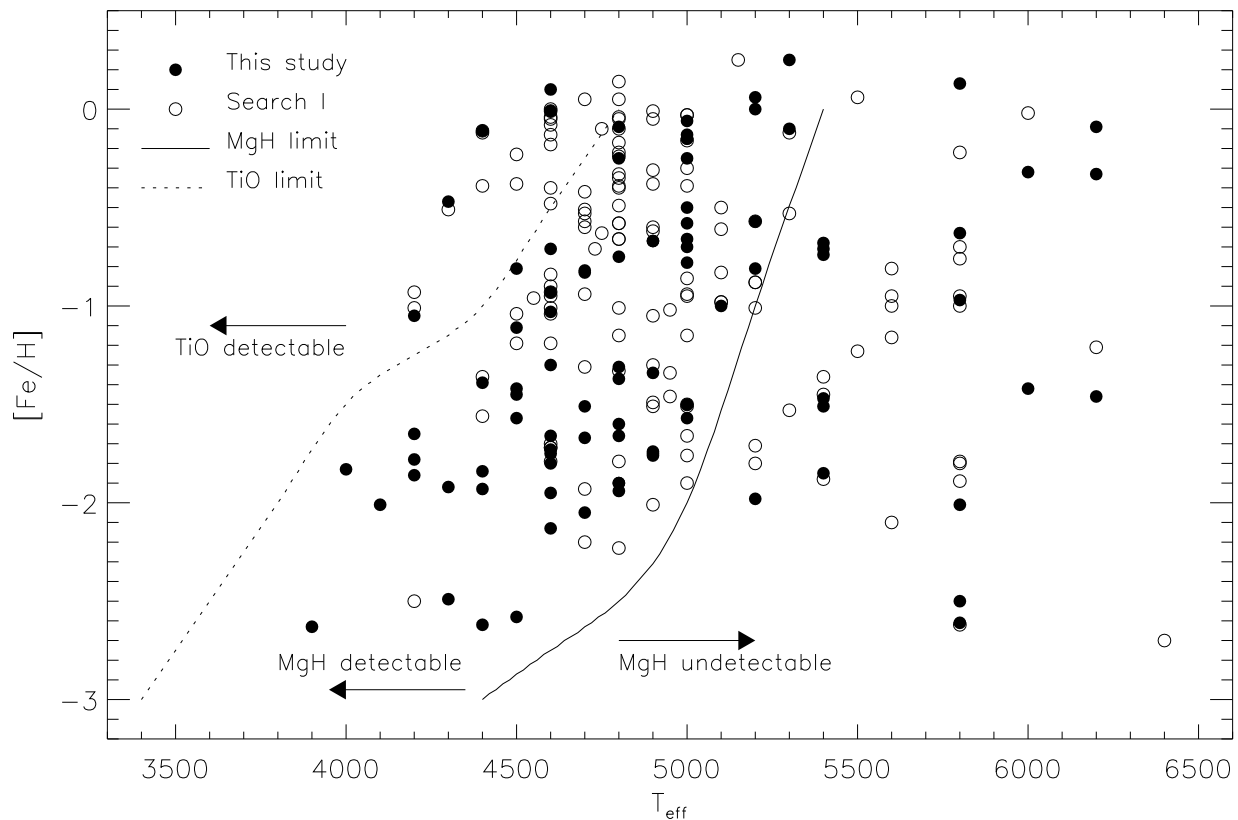


Fig. 5.— Limit of detection for MgH and TiO features based on spectral synthesis of representative lines assuming $\log g = 4.5$ and $R=60,000$. The filled circles are from this study while the open circles are from Paper I. With the exception of a few stars from Paper I, all stars with MgH lines lie to the left of the MgH detection limit. Also, all stars without MgH lines lie to the right of the MgH detection limit. The few stars that do not lie where they ought to are giants or were observed at lower resolving powers.

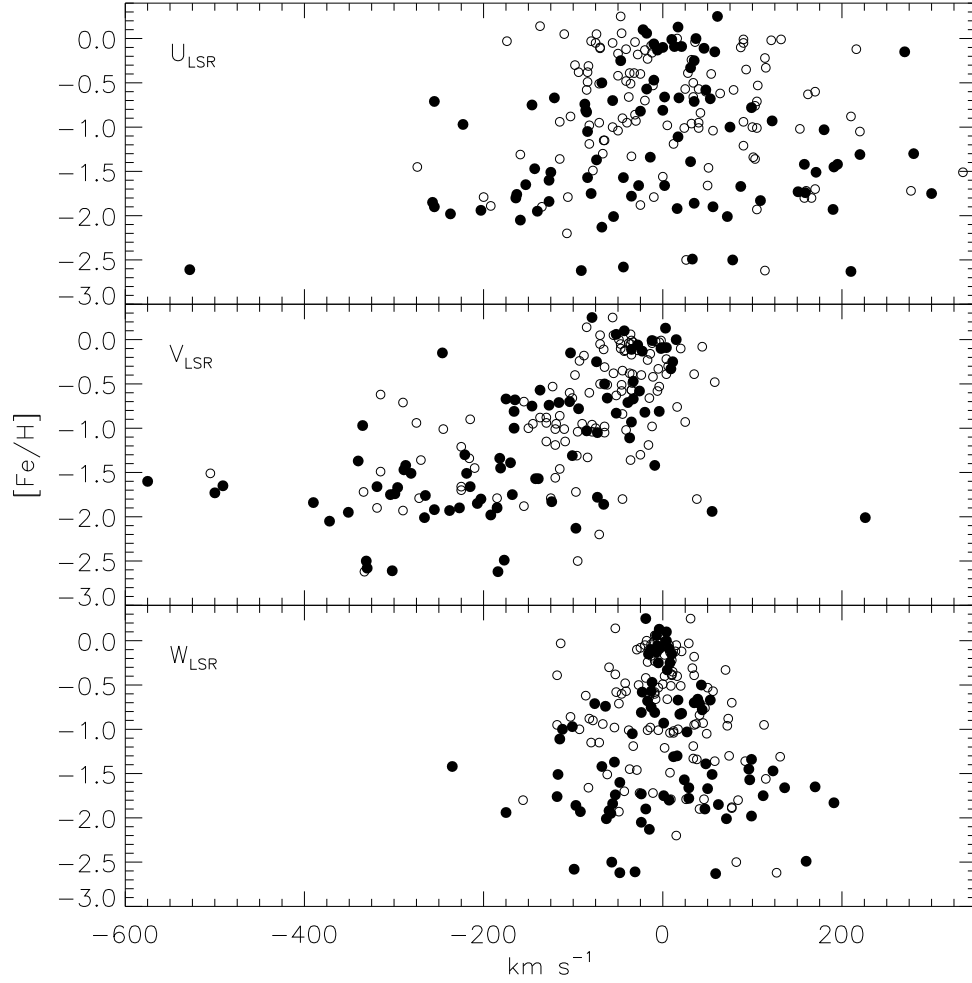


Fig. 6.— Galactic space-velocity U , V , and W (relative to the LSR) vs $[\text{Fe}/\text{H}]$. The open circles represent the data from Paper I while the filled circles are stars from this study. Only stars which have $\frac{\sigma_U + \sigma_V + \sigma_W}{|U| + |V| + |W|} < 0.7$ are shown. A considerable fraction of the sample noticeably lag the LSR ($V < -50$ km/s).

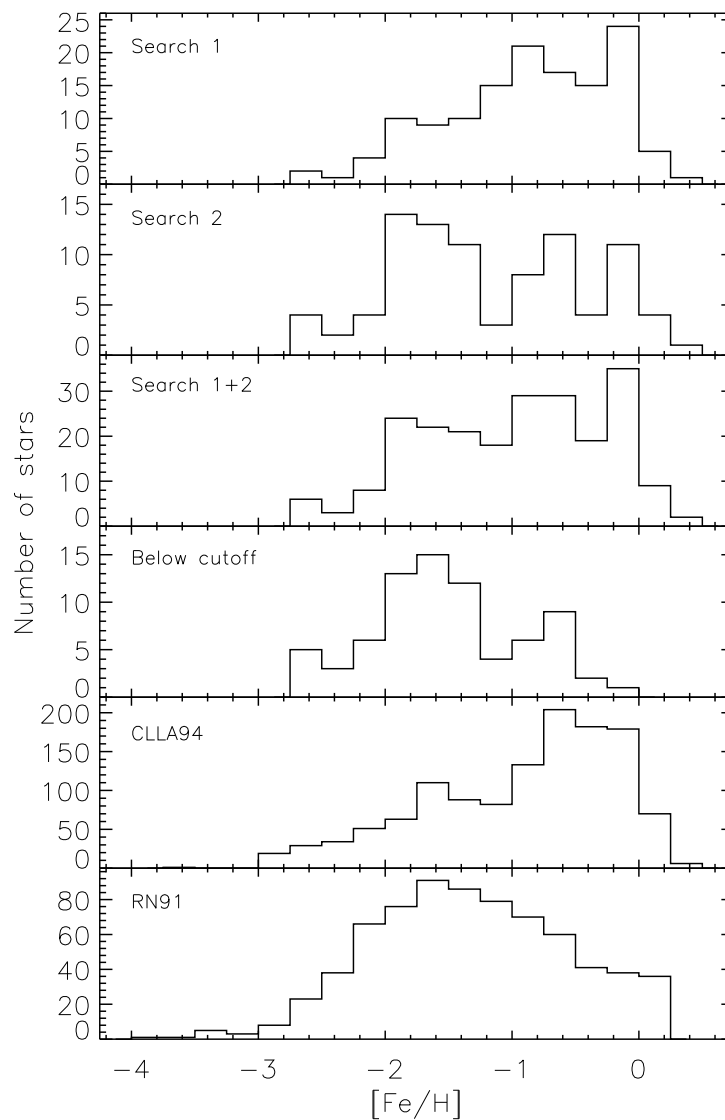


Fig. 7.— Number of stars versus metallicity for Paper I (top panel), this study (2nd panel), Paper I and this study (3rd panel), only the stars falling below the cutoff defined in Figure 1 (4th panel), the Carney et al. (1994) study (5th panel), and the Ryan & Norris (1991) study (bottom panel). The 4th panel shows most clearly that our selection technique efficiently selects metal-poor stars.

Fig. 8.— $V - J$ reduced proper motion diagram based on the Salim & Gould (2002) photometry. In each panel, the small dots are stars in the NLTT catalog with 2MASS and USNO photometry. We overplot (large circles) the locations of stars we previously observed for which we were able to derive metallicities either in this study or in Paper I. In the upper left panel the large circles are stars with $[\text{Fe}/\text{H}] < -1.5$, in the upper right panel are stars with $-1.5 < [\text{Fe}/\text{H}] < -1.0$, in the lower left panel are stars with $-1.0 < [\text{Fe}/\text{H}] < -0.5$, and in the lower right panel are stars with $[\text{Fe}/\text{H}] > -0.5$. The dotted and dashed lines (based on Samir & Gould) define approximate boundaries between main sequence stars (MS), subdwarfs (SD), and white dwarfs (WD). In the upper left panel, the stars with $[\text{Fe}/\text{H}] < -2.0$ (open circles) overlap with the $[\text{Fe}/\text{H}] < -1.5$ stars.

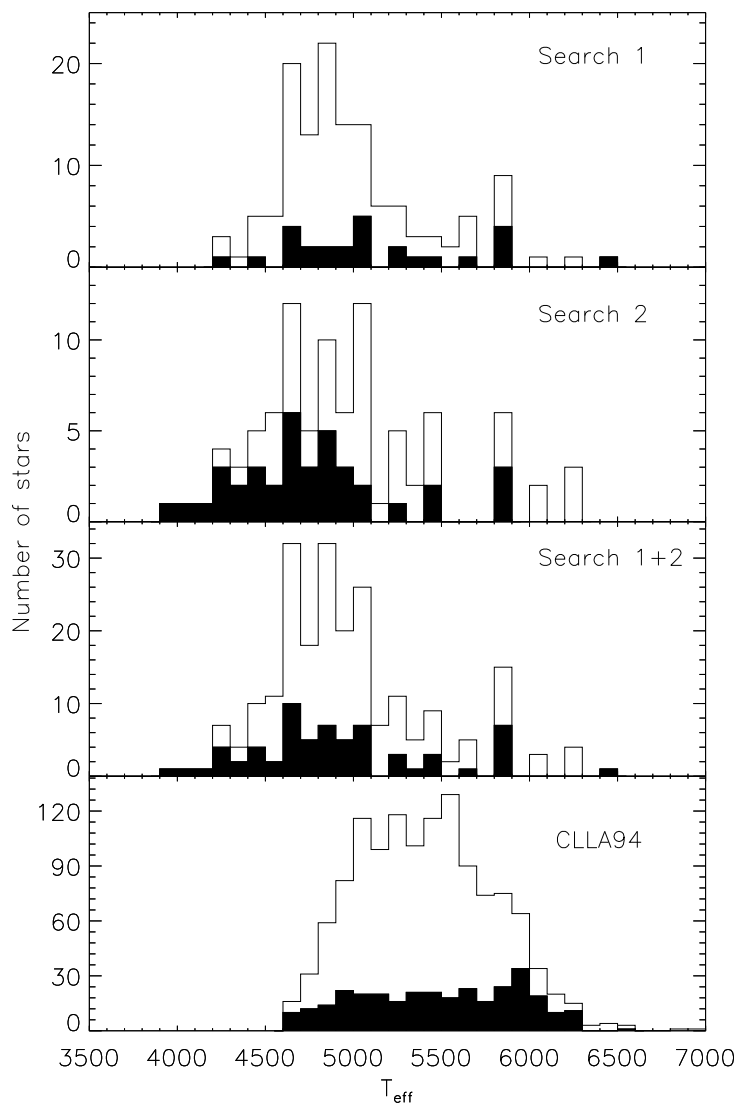


Fig. 9.— Number of stars versus effective temperature for Paper I (top panel), this study (2nd panel), Paper I and this study (3rd panel), and the Carney et al. (1994) study (bottom panel). The filled histograms represent the distribution of stars with $[\text{Fe}/\text{H}] \leq -1.5$. Clearly our samples peak at lower values of T_{eff} than the Carney sample. The 2nd panel shows that our selection technique is very efficient at identifying cool stars with $[\text{Fe}/\text{H}] \leq -1.5$.

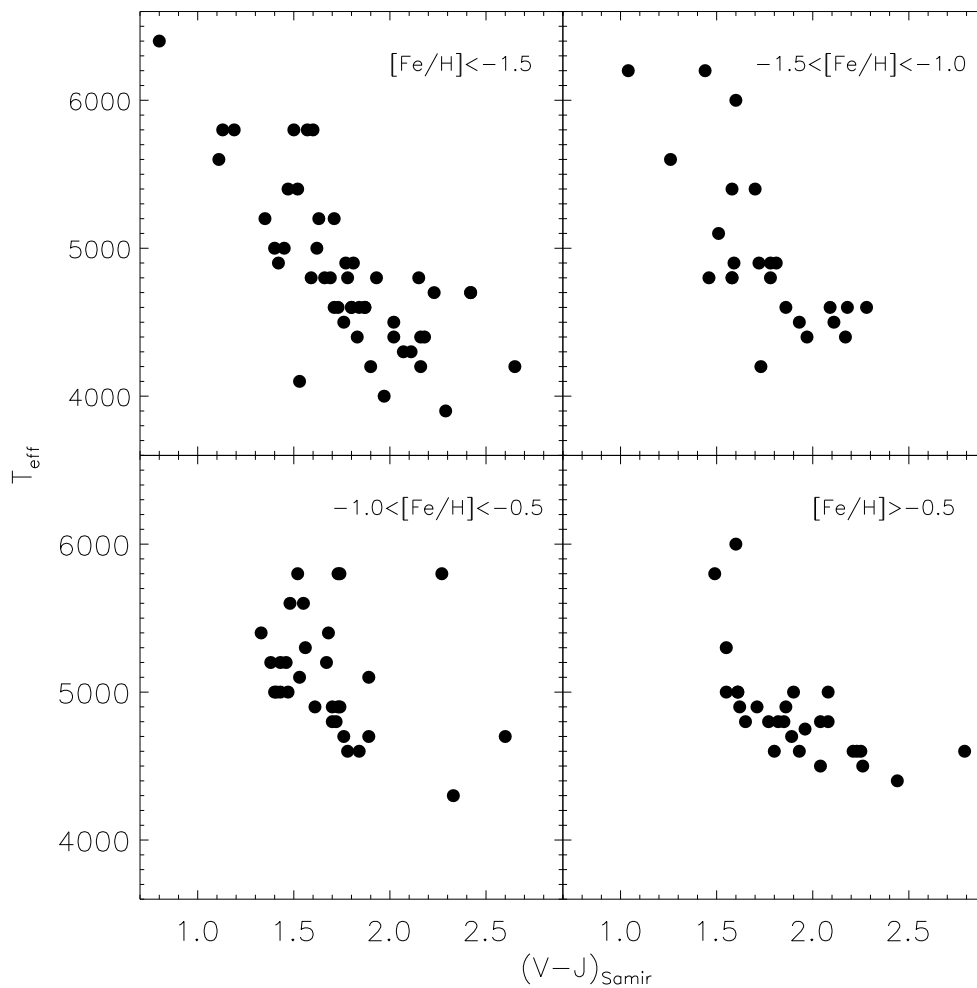


Fig. 10.— $V - J$ color from Salim & Gould (2002) versus effective temperature derived from this study and Paper I. In the upper left panel are stars with $[\text{Fe}/\text{H}] < -1.5$, in the upper right panel are stars with $-1.5 < [\text{Fe}/\text{H}] < -1.0$, in the lower left panel are stars with $-1.0 < [\text{Fe}/\text{H}] < -0.5$, and in the lower right panel are stars with $[\text{Fe}/\text{H}] > -0.5$. Given a value of $V - J$, the corresponding T_{eff} can be determined with reasonable accuracy.

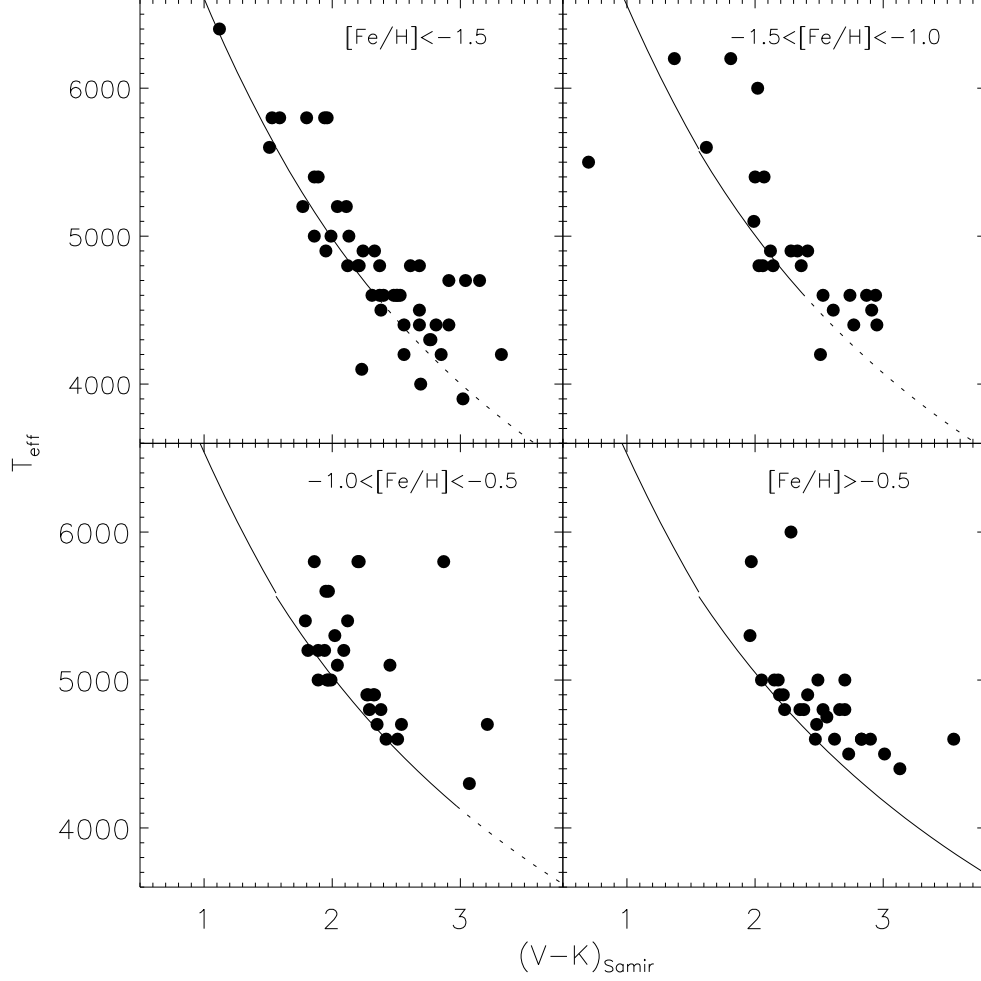


Fig. 11.— $V - K$ color from Salim & Gould (2002) versus effective temperature derived from this study and Paper I. In the upper left panel are stars with $[\text{Fe}/\text{H}] < -1.5$, in the upper right panel are stars with $-1.5 < [\text{Fe}/\text{H}] < -1.0$, in the lower left panel are stars with $-1.0 < [\text{Fe}/\text{H}] < -0.5$, and in the lower right panel are stars with $[\text{Fe}/\text{H}] > -0.5$. In each panel, the solid line is the $(V - K):T_{\text{eff}}$ relation from Alonso et al. (1996) for dwarfs. The dotted line is the extrapolation of the $(V - K):T_{\text{eff}}$ relation.

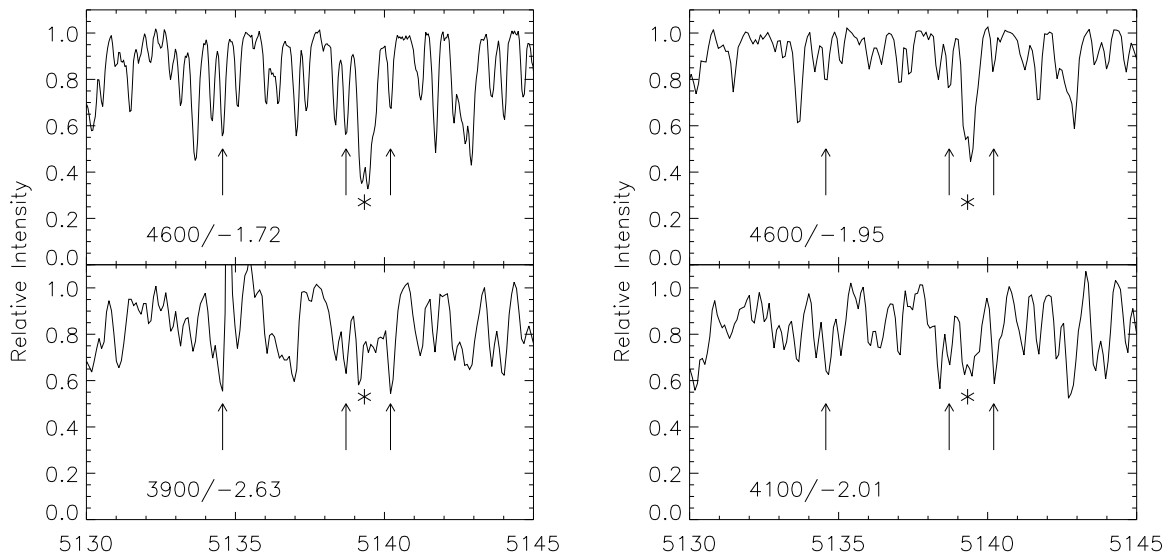


Fig. 12.— Observed spectra of 4 different cool subdwarfs. The effective temperature and metallicity of each star is shown. In each panel, the 3 arrows highlight representative MgH lines while the asterisk highlights an atomic line (Fe and Ni). In the upper panels, the 3 MgH lines are dwarfed by the strong atomic line. In the lower panels, the 3 MgH lines are of comparable strength to the atomic line.

Table 1. Basic data and derived parameters for objects

Name	Ra ^a	Dec ^b	T _{eff}	[Fe/H]	log g	ξ_t	U _{LSR}	σ_U	V _{LSR}	σ_V	W _{LSR}	σ_W	Molecular	Source
	2000	2000	(K)		(cm s ⁻²)		(km/s)						Features	
LP 644-47	820	-51448	5400	-1.47	4.5	0.8	-163	83	-294	93	116	38	N	Samir02
NLTT 718	1445	412237	4800	-0.75	4.5	0.2	-166	109	-151	61	-20	21	Y	Samir02
G 31-56	2947	10112	4600	-0.93	4.5	0.3	102	36	-40	20	-6	15	Y	Sandage86
LP 705-100	3613	-84036	5400	-0.74	4.5	0.8	-107	63	-132	81	-71	18	Y	Samir02
LP 705-89	4243	-123918	5800	-0.97	4.5	0.6	-243	110	-340	155	-108	25	N	Samir02
G 69-18	4432	295424	4500	-2.58	4.5	0.3	-64	44	-335	70	-106	58	Y	Samir02
G 1-19	4449	-642	4200	-1.78	4.5	0.3	-55	22	-78	19	22	3	Y	Sandage86
LP 882-323	10956	-300853	4100	-2.01	4.5	0.4	-75	15	221	37	64	3	Y	Samir02
HIP 6001	11711	93004	4600	-0.71	4.5	0.3	15	4	-44	5	34	1	Y	Hipp
G 272-38	13303	-161100	4400	-1.39	4.5	1.1	11	6	-175	67	41	3	Y	Samir02
G 72-18	13756	322100	4900	-1.74	4.5	0.4	139	10	-304	77	-60	87	Y	Samir02
G 3-13	14258	170802	4700	-1.67	4.5	0.6	67	20	-301	78	43	36	Y	Sandage86
HIP 8775	15251	44958	4600	-0.01	4.5	0.8	-10	3	-17	3	-4	1	Y	Hipp
LP 829-11	20514	-202942	4900	-1.34	4.5	0.3	-34	34	-187	101	92	19	Y	Samir02
LP 829-30	21348	-253100	4600	-1.73	4.5	0.8	131	50	-505	170	-31	17	Y	Samir02
G 3-44	21350	155910	4200	-1.65	4.5	0.4	-173	90	-496	134	163	16	Y	Samir02
NLTT 7419	21426	-245707	5000	-1.57	4.5	0.5	-64	17	-144	36	17	11	Y	Samir02
HIP 10682	21727	270814	5000	-0.15	4.5	0.5	38	3	-108	9	3	5	Y	Hipp
LP 885-44 ^c	21738	-320430	4900	-0.67	4.5	0.4	-141	47	-38	11	10	12.8	Y	Samir02
G 74-21	22415	411348	4700	-1.51	4.5	0.5	-145	82	-286	97	48	12	Y	Samir02
LP 770-34	23130	-153648	4500	-1.45	4.5	0.3	171	35	-186	65	89	10	Y	Samir02
G 75-23	23321	-64354	5400	-1.51	4.5	0.6	151	73	-224	106	-124	48	N	Samir02
G 75-32	23935	-51436	5000	-0.7	4.5	0.4	-76	22	-109	33	28	14	Y	Samir02
LP 887-18	25827	-290428	4400	-1.93	4.5	0.6	170	63	-243	65	-99	3	Y	Samir02
HIP 14803	31110	91147	4600	0.1	4.5	0.7	-42	4	-48	8	-3	3	Y	Hipp
G 5-26	31753	233720	4800	-1.6	4	0.5	-147	59	-580	214	-55	22	Y	Samir02
LP 772-56	32353	-171822	4400	-1.84	4.5	0.4	-147	9	-395	88	-63	33	Y	Samir02
HIP 16739	33519	54331	4500	-0.81	4.5	0.6	-20	1	-9	3	-31	2	Y	Hipp
LP 773-20	33903	-192636	5000	-0.78	4.5	0.6	79	18	-99	38	37	5	Y	Samir02
HIP 17451	34427	-4114	5800	0.13	4.5	0.8	-3	1	-2	1	-11	1	N	Hipp
G 39-1 ^c	40734	380430	5000	-0.06	4.5	1.1	-30	2	-28	6	-6	2	Y	CLLA94
HIP 19814	41458	-53749	5400	-0.71	4.5	1	-275	58	-121	45	-83	90	Y	Hipp
HIP 21380 ^c	43517	230243	5300	-0.1	4.5	1.1	-20	1	-2	1	-13	1	Y	Hipp
G 8-45	43749	194018	4200	-1.05	4.5	0.7	-104	1	-78	15	-41	3	Y	Samir02
G 83-26	43816	125100	4500	-1.57	4.5	0.6	-104	9	-147	32	90	28	Y	Sandage86
G 83-46	45623	145510	4400	-2.62	4.25	0.3	-111	4	-189	36	-55	4	Y	Sandage86
WT 1428	45729	-235723	4900	-1.76	4.5	0.4	-183	4	-270	24	-125	22	Y	Samir02
HIP 23113	45824	514935	6200	-0.09	4.25	1	-7	2	-1	3	0	2	N	Hipp
HIP 23198	45932	484645	4300	-0.47	4.5	0.8	-30	2	-38	4	-19	2	Y	Hipp
HIP 24289	51245	41916	5000	-0.66	4.5	1.1	-18	1	-67	10	32	8	Y	Hipp
HIP 24655	51726	260449	6200	-0.33	3.5	2.1	11	2	5	3	-3	3	N	Hipp
NLTT 14937	52211	351726	4900	-1.75	4.5	0.3	-100	11	-168	78	1	7	Y	Samir
HIP 26864	54213	72407	4500	-1.11	4.5	0.4	-3	4	-42	3	-122	14	Y	Hipp
G 249-37 ^c	60625	635007	5000	-0.13	4.5	0.8	-26	1	-23	1	-7	1	Y	CLLA94
HIP 29316	61055	101905	4400	-0.11	2	1.9	26	1	-40	2	-20	1	Y	Hipp
LP 720-6	62238	-125305	4600	-1.75	4.5	0.3	280	76	-309	96	105	30	Y	Samir02
LP 661-1	64854	-45907	5200	-1.98	4.5	0.5	-257	101	-192	138	99	48	N	Samir
HIP 33848 ^c	70136	65537	5200	0	4.5	0.8	17	1	15	1	4	1	Y	Hipp
NLTT 17752 ^c	72132	-202041	5800	-2.01	4	0.4	52	53	-271	36	-70	21	N	Samir02
HIP 36827 ^c	72436	-65348	5000	-0.25	4.5	1.1	15	1	11	1	-5	1	Y	Hipp
G 87-38	72819	375631	5800	-0.63	4.5	0.7	195	177	-1398	1462	354	369	Y	Samir
G 40-5 ^c	80435	152151	5200	0.06	4.5	0.8	-38	1	-52	1	-7	2	Y	CLLA94
G 51-7	82007	344212	4600	-1.66	4.5	0.7	-47	6	-215	91	29	10	Y	Samir
HIP 42145 ^c	83528	414425	4800	-0.25	4.5	0.6	-67	1	-74	3	8	1	Y	HIPP(vel)
G 9-13 ^c	83951	113122	5000	-0.58	4.5	0.5	28	1	-26	1	-23	1	Y	CLLA94
HIP 44526 ^c	90421	-155451	4800	-0.09	4.5	1	1	1	-1	1	-4	1	Y	HIPP(vel)
NLTT 20889	90446	392419	5800	-2.5	4.5	1	58	14	-331	176	-57	23	N	Samir
G 41-29	91419	200136	4300	-2.49	4.5	0.4	13	39	-177	42	160	17	Y	Samir
G 116-51	94617	383918	4900	-0.67	4.5	0.7	-2	11	-175	74	53	13	Y	Samir
G 43-30 ^c	101008	181113	5300	0.25	4.5	0.8	41	3	-79	7	-19	2	Y	CLLA94
G 54-29	102854	270229	4700	-2.05	4	0.4	-179	56	-372	160	-24	72	Y	Samir02
LP 612-37	111935	-32750	4000	-1.83	4.5	0.3	89	6	-124	16	191	5	Y	Samir02
HIP 56461 ^c	113436	400923	4800	-1.37	4.5	0.4	-94	33	-345	94	-61	5	Y	Samir02
LP 319-42	115232	273051	4600	-1.8	4.5	0.4	-184	45	-203	26	7	50	Y	Samir02
LHS 343	125624	154143	3900	-2.63	4	0.5	190	60	-625	230	59	44	Y	Samir02

Table 1—Continued

Name	Ra ^a	Dec ^b	T _{eff}	[Fe/H]	log g	ξ_t	U _{LSR}	σ_U	V _{LSR}	σ_V	W _{LSR}	σ_W	Molecular Features	Source
	2000	2000	(K)		(cm s ⁻²)		(km/s)							
ROSS 471	132041	-122606	4600	-2.13	4.5	0.5	-88	37	-97	43	-15	6	Y	Samir02
G 63-40	133648	190513	4600	-1.95	4.5	0.3	-160	55	-351	134	-58	12	Y	Samir02
NLTT 35929	135935	224757	5200	-0.57	4.5	0.5	-38	21	-137	77	-13	14	Y	Samir02
G 136-67	150816	150948	5000	-0.5	4.5	0.6	-88	22	-65	18	43	18	Y	Samir02
G 181-19	165910	345200	4800	-1.66	4.5	0.3	-18	13	-324	71	129	70	Y	Samir02
G 140-16	175248	143837	6000	-0.32	3.75	1.4	842	754	-835	689	-471	390	N	Samir02
LP 393-3	193307	235951	4300	-1.92	4.5	0.7	-4	21	-260	12	-67	12	Y	Samir02
G 23-7	193544	14342	5400	-0.68	4.5	0.6	33	20	-170	26	-24	8	Y	Sandage86
LP 813-13	194343	-155524	6000	-1.42	4.5	1	138	31	-292	83	-75	22	N	Samir02
HIP 97174	194503	291943	4700	-0.83	4.5	0.3	-105	6	-57	3	12	2	Y	Hipp
NLTT 48700	200516	311210	4800	-1.9	4.5	0.2	-275	4	-232	50	40	37	Y	Samir02
G 231-39	211833	522336	4600	-1.3	4.5	0.3	260	58	-226	4	9	6	Y	Samir02
NLTT 51106	212214	-270217	4800	-1.94	4.5	0.4	-223	90	50	18	-182	67	Y	Samir02
G 126-2	212907	121059	4500	-1.42	4.5	0.9	175	32	-14	38	-242	1	Y	Sandage86
LP 873-63	213139	-214812	5100	-1	4.5	0.3	55	7	-171	79	-119	34	Y	Samir02
WT 2218	220744	-221453	6200	-1.46	4.5	1	-336	232	-275	228	-116	162	N	Samir02
LP 759-73	221840	-100812	5400	-1.85	4.5	0.9	-277	62	-212	29	55	51	N	Samir02
LP 875-62	222601	-205031	4600	-1.03	4.5	0.4	160	57	-90	35	20	8	Y	Samir02
HIP 112486	224704	295108	5000	-1.5	4.5	0.5	-2045	6852	-1104	2808	-1412	5086	Y	Samir02
NLTT 55528	230013	215631	5800	-2.61	4.5	1	-548	351	-307	77	-38	89	N	Samir02
G 273-76	233457	-203854	4800	-1.9	4.5	0.2	36	25	-190	61	-26	15	Y	Samir02
G 157-88	233757	-74542	5000	-0.15	4.5	0.6	250	140	-251	127	-23	46	Y	Samir02
G 273-105	234117	-194748	4800	-1.31	4.5	0.5	200	84	-106	48	5	4	Y	Samir02
G 266-8	235614	-262559	5200	-0.81	4.5	0.3	-106	28	-171	42	-16	10	Y	Samir02
G 30-31	235754	83646	4200	-1.86	4.5	0.4	15	13	-71	23	-104	18	Y	Sandage86
G 129-57 ^c	235831	203424	4700	-0.82	4.5	0.3	-45	10	-25	3	14	2	Y	Sandage86

^ahhmmss

^bddmmss

^cData taken with R=60000

References. — (CLLA94) = Carney et al. (1994); (Hipp) = HIPPARCOS catalog; (NLTT) = Salim & Gould (2002); (Sandage86) = Sandage & Kowal (1986)

Table 2. Comparison with literature

Star	This study		Literature		Source
	T _{eff}	[Fe/H]	T _{eff}	[Fe/H]	
LP 644-47	5400	-1.47		-2.07	RN91
	5400	-1.47	5341	-1.63	CLLA94
LP 705-89	5800	-0.97		-1.12	RN91
G 72-18	4900	-1.74	4982	-1.86	CLLA94
G 39-1	5000	-0.06	4867	-0.61	CLLA94
HIP 19814	5400	-0.71	5378	-0.69	CLLA94
G 83-26	4500	-1.57		-2.30	RN91
HIP 24289	5000	-0.66	5032	-0.77	CLLA94
G 249-37	5000	-0.13	4954	-0.27	CLLA94
LP 661-1	5200	-1.98		-2.03	RN91
G 40-5	5200	0.06	5012	-0.07	CLLA94
G 9-13	5000	-0.58	5049	-0.27	CLLA94
G 43-30	5300	0.25	5070	-0.21	CLLA94
G 181-19	4800	-1.66	4892	-1.56	CLLA94
LP 813-13	6000	-1.42		-2.10	RN91
LP 873-63	5100	-1.00		-0.83	RN91
LP 759-73	5400	-1.85		-1.63	RN91
G 273-105	4800	-1.31		-2.17	RN91

References. — (CLLA94) = Carney et al. (1994); (RN91) = Ryan & Norris (1991);

This figure "fig1.jpeg" is available in "jpeg" format from:

<http://arxiv.org/ps/astro-ph/0306076v1>

This figure "fig8.jpeg" is available in "jpeg" format from:

<http://arxiv.org/ps/astro-ph/0306076v1>